International Journal of Minerals, Metallurgy and Materials
Volume 26, Number 8, August 2019, Page 938
https://doi.org/10.1007/s12613-019-1810-0

Migration behaviors and kinetics of phosphorus during coal-based reduction of high-phosphorus oolitic iron ore

Yong-sheng Sun, Yan-feng Li, Yue-xin Han, and Yan-jun Li

School of Resources and Civil Engineering, Northeastern University, Shenyang 110819, China
(Received: 24 August 2018; revised: 11 March 2019; accepted: 12 March 2019)

Abstract: To understand the migration mechanisms of phosphorus (P) during coal-based reduction, a high-phosphorus oolitic iron ore was reduced by coal under various experimental conditions. The migration characteristics and kinetics of P were investigated by a field-emission electron probe microanalyzer (FE-EPMA) and using the basic principle of solid phase mass transfer, respectively. Experimental results showed that the P transferred from the slag to the metallic phase during reduction, and the migration process could be divided into three stages: phosphorus diffusing from the slag to the metallic interface, the formation of Fe–P compounds at the slag–metal interface and P diffusing from the slag–metal interface to the metallic interior. The reduction time and temperature significantly influenced the phosphorus content of the metallic and slag phases. The P content of the metallic phase increased with increasing reduction time and temperature, while that of the slag phase gradually decreased. The P diffusion constant and activation energy were determined and a migration kinetics model of P in coal-based reduction was proposed. P diffusion in the metallic phase was the controlling step of the P migration.

Keywords: high-phosphorus oolitic iron ore; coal-based reduction; phosphorus migration; kinetics

1. Introduction

Refractory iron ores have become increasingly important with the rapid depletion of high-quality iron ore [1–2]. The most representative refractory iron ore is oolitic iron ore, which is widely distributed in France, Canada, Nigeria, the United Kingdom, Saudi Arabia, the Israel-Lebanon border, Algeria, and China [3–4]. However, oolitic iron ore is currently unexploited and considered to be the most abundant refractory iron ore in the world due to its complex mineral composition, special concentric oolitic texture and high-phosphorus (P) content (0.4wt%–1.8wt%) [5–6].

Recently, numerous methods, such as physical separation [7], flotation [8–9], bio-leaching [10], chemical leaching [11–12], magnetic roasting–magnetic separation [13–14], and coal-based reduction–magnetic separation [2,5,15–16], have been developed for processing oolitic iron ore. Previous studies indicate that a coal-based reduction–magnetic separation process is the most feasible method to recover iron from oolitic iron ore. However, the large amount of apatite in the ore is reduced to P and then transferred into the metallic iron during coal-based reduction. It is well known that P is a detrimental impurity in steelmaking and the P content of the feed stock for steelmaking must be strictly controlled.

Excellent studies have been conducted on the removal and distribution of P in coal-based reduction. Yu *et al.* [17] reported that $Ca(OH)_2$ and Na_2CO_3 additives restrained the reduction of fluorapatite, and metallic iron with 93.28wt% Fe and 0.07wt% P was obtained at 92.30% recovery. Some researchers [18–19] investigated the distribution characteristics of P and determined it is present in the form of Fe_3P in iron ore. Cha *et al.* [1] clarified the distribution behavior of P under various experimental conditions during the reduction of high-P iron ore. Without prior P removal, an innovative method was proposed to simultaneously recover iron and P from high-phosphorus oolitic iron ore [20–24]. During reduction, P enriches the metallic iron phase, and the P-rich metallic iron is separated from slag by magnetic separation. The P-rich metallic iron can be directly used as

Corresponding author: Yong-sheng Sun E-mail: yongshengsun@mail.neu.edu.cn

feed material for high-phosphorus steel [20] or treated in a dephosphorization process to obtain low P hot metal and phosphate fertilizer (i.e., high-phosphorus slag) [21–24]. Most studies have focused on the dephosphorization and distribution of P. However, the migration behavior of P into the metallic iron phase, which is imperative for controlling P enrichment, has not been clarified.

The present study aims to study the migration mechanisms of P during coal-based reduction. A high-phosphorus oolitic iron ore was reduced by coal under different reduction time and temperatures. The P content at different positions in the reduced ore was analyzed using FE-EPMA. The migration behaviors and kinetics of P were investigated.

2. Experimental

2.1. Materials

A high-phosphorus oolitic iron ore sample from Hubei Province of China was used. The chemical composition (Table 1) of the ore sample is 42.21wt% iron, 1.31wt% P, 21.80wt% SiO_2, 5.47wt% Al_2O_3 and 4.33wt% CaO. The XRD pattern in Fig. 1 indicates that the ore mainly contains hematite, quartz, chamosite, and apatite. The photomicrograph of raw ore detected by a mineral liberation analyzer (MLA) is shown in Fig. 2. The hematite, chamosite and apatite phases are closely associated with each other and form the concentric oolitic structure, which indicates that the ore sample is a typical oolitic iron ore. Coal used as the reductant was obtained from the Jilin Province of China. As shown in Table 2, the coal consists of 67.83wt% fixed carbon, 18.45wt% volatiles, 12.02wt% ash and 1.48wt% moisture. The P and S contents in the coal are very low. The iron ore and coal were both crushed to 100% passing 2 mm. The particle size distributions of the crushed samples are shown in Table 3, indicating the particle size of iron ore and coal was mainly distributed in the range of 0.074–2 mm.

Table 1. Chemical composition of the high-phosphorus oolitic iron ore wt%

Total Fe	FeO	SiO_2	Al_2O_3	CaO	MgO	P	S
42.21	4.31	21.80	5.47	4.33	0.59	1.31	0.03

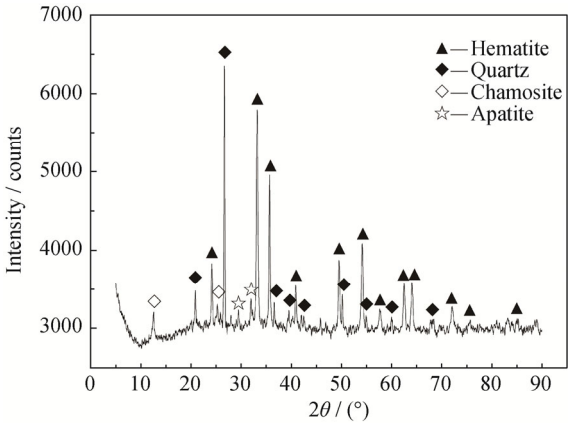

Fig. 1. XRD pattern of the high-phosphorus oolitic iron ore.

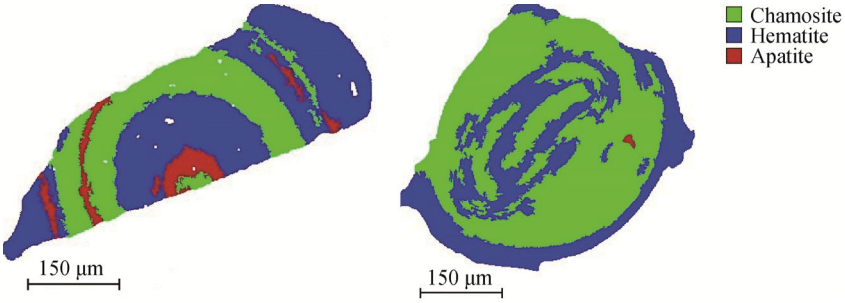

Fig. 2. MLA detection images of the raw ore.

Table 2. Proximate analysis of the coal wt%

Fixed carbon	Volatile matter	Ash	Moisture	P	S
67.83	18.45	12.02	1.48	0.004	0.028

2.2. Experimental procedure

Reduction experiments were performed in a KSL-1400X electric resistance furnace. With a pre-determined C/O molar ratio (i.e., molar ratio of fixed carbon in the coal to reducible oxygen in iron oxides) of 2.0, the crushed iron ore and coal were homogeneously mixed, and 100 g of the mixture was charged into an alumina crucible (150 ml). The crucible was then placed in a furnace with a target temperature of 1473, 1498, 1523, or 1548 K. After a 10, 20, 30, 40, 60, or 80 min, the crucible was taken out and cooled down to room temperature by quenching in water. The wet reduced sample was subsequently filtered and dried at 353 K in a vacuum oven. The obtained reduced sample was analyzed by FE-EPMA.

Table 3. Particle size distributions of the oolitic iron ore and coal wt%

Materials	1−2 mm	0.5−1 mm	0.074−0.5 mm	0.045−0.074 mm	< 0.045 mm	Total
Oolitic iron ore	19.45	26.15	44.95	4.83	4.62	100
Coal	16.46	40.24	36.56	2.63	4.11	100

2.3. FE-EPMA analysis

The P content at different positions of the metallic iron and slag phases in the reduced sample was determined by a JEOL JXA-8530F field-emission electron probe microanalyzer (FE-EPMA). The detection process is shown in Fig. 3. The reduced sample was fixed by epoxy resin and polished to form a cross section. Field-emission scanning electron microscopy (FESEM) was used to find the target area containing slag and metallic iron phases in the cross section, and a wavelength dispersive spectrometer (WDS) was used to detect the P content. Six different micro-size areas were analyzed for each sample, and the P content at seven different positions was detected in each area (as shown in Fig. 3). The average value of the P content at the corresponding position was used as the experimental data. The obtained data were presented in a figure, which was plotted with the P content as the Y-axis, the position as the X-axis, and the interface between the metallic iron and slag phases as the origin (the interior of the metal is positive, the interior of the slag is negative).

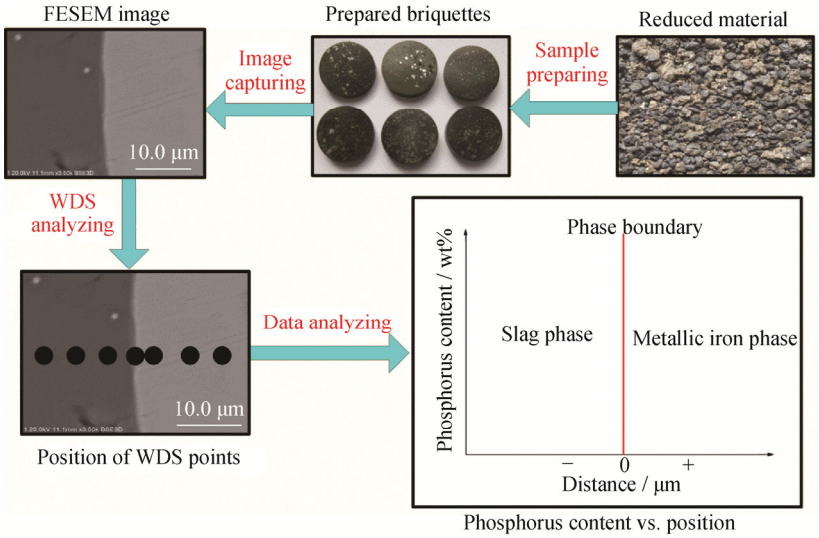

Fig. 3. Schematic diagram for detection of phosphorus.

3. Results and discussion

3.1. Migration route of phosphorus

For a closer look at the P migration behavior, the reduced sample prepared at 1523 K for 40 min was observed by line scanning of EPMA, and the results are shown in Fig. 4. Metallic iron and slag phases were clearly observed in the reduced ore. The Fe-line scanning revealed that the iron content of the metallic phase approached 100wt%, while the iron content of the slag phase was comparatively low, indicating that iron minerals in the ore were reduced to metallic iron and formed the metallic iron phase. The P-line scanning showed that the P content in the metallic phase was much higher than that in the slag phase, indicating that P effectively enriched the metallic iron phase during reduction. Additionally, the P content in the boundary region of the metallic phase was higher than that in the internal region. With the line scanning position moving from the edge to the inside of the metallic phase, the P content decreased and gradually reached a stable value.

A previous study similarly found that the P content in the metallic iron decreased from the edge to the center and presented as a solid solution of α-Fe and Fe_3P in the metallic iron phase [18]. According to the change in P and its existing form in the metallic phase, the migration route of P during reduction was as follows. A large amount of metallic iron was generated prior to the reduction of P, which provided a matrix for P enrichment. The reduced P migrated from the slag to the slag–metal interface and reacted with metallic iron to form an Fe–P compound in the slag–metal interface; furthermore, P gradually diffused from the interface to the interior of the metallic phase under the concentration gradient and existed as a solid solution of the metal phase.

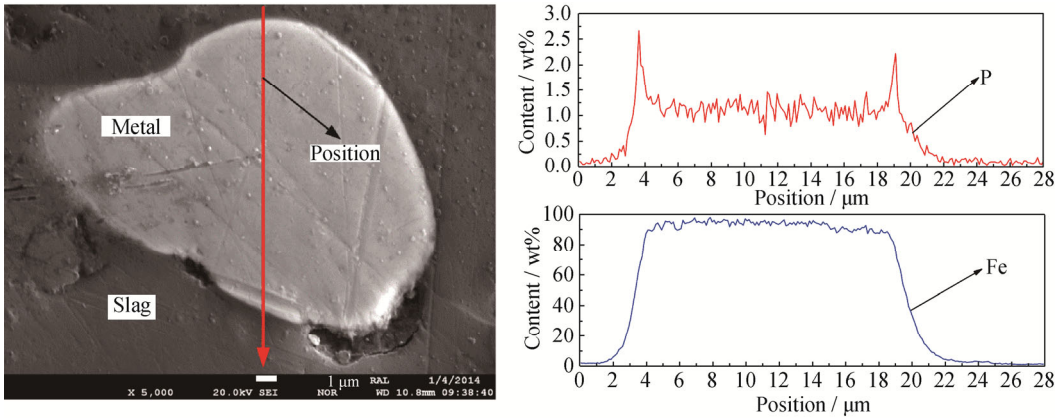

Fig. 4. EPMA line scanning of the sample reduced at 1523 K for 40 min.

3.2. Migration characteristics of phosphorus

High-phosphorus oolitic iron ore was reduced under different experimental conditions. The P content at different positions is shown in Fig. 5. The phosphorus content at different positions in a metallic phase or slag phase presented a similar variation under different reduction temperatures and time. The phosphorus content gradually decreased from the metallic phase boundary to the interior, while the phosphorus content gradually increased from the interior of the slag phase to the slag–metal interface. For example, at a reduction temperature of 1523 K and a reduction time of 10 min, the P content at the −5 μm and −1 μm positions in the slag phase was 1.08wt% and 1.23wt%, respectively, while the P content at the 0 μm position in the metallic phase was 1.06wt% and decreased to 0.68wt% at the 5 μm position. This result is consistent with previous scanning analysis results (Fig. 4), which further proved that the P was transferred from the slag to the metal phase during the reduction process and gradually enriched in the metal phase.

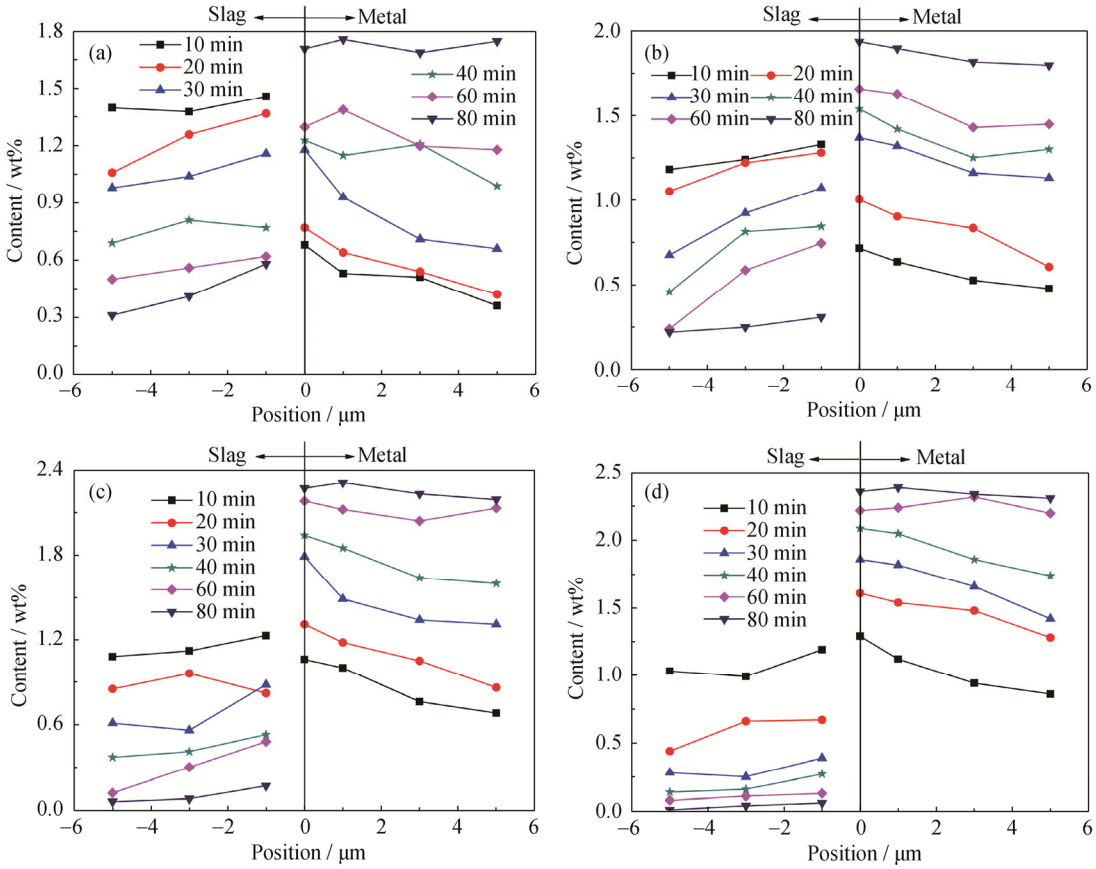

Fig. 5. Phosphorus content at different positions of samples reduced at (a) 1473 K, (b) 1498 K, (c) 1523 K, and (d) 1548 K.

The reduction time had a significant influence on the P content at different positions. At the same reduction temperature and detected position, the P content in the slag decreased significantly with increasing reduction time, while the P content in the metal phase increased rapidly. For instance, when the reduction time increased from 10 to 80 min at a reduction temperature of 1498 K, the P content at the −5 μm position in the slag phase decreased from 1.19wt% to 0.22wt%, while the P content at the 5 μm position in the metallic phase increased from 0.48wt% to 1.81wt%. The reason for this behavior is that more apatite in the ore was reduced to P with more reduction time, and more P transferred into the metallic phase. In addition, the extension of reduction time provided more time for the transfer of P from the slag to the metallic phase.

As shown in Fig. 5, the reduction temperature also had a significant effect on the P content at different positions. At the same reduction time and detected position, the P content of the slag phase showed a decreasing trend with increasing reduction temperature, while the P content of the metallic phase increased. For example, when the reduction time was 20 min, as the reduction temperature increased from 1473 K to 1548 K, the P content at the −3 μm position in the slag phase decreased from 1.26wt% to 0.66wt%, while the content at the 3 μm position in the metal phase increased from 0.54wt% to 1.48wt%. This behavior is attributed to the high reduction temperature accelerating the reduction of apatite [1]. Additionally, the random movement of molecules will be intensified by increasing temperature, which benefits P migration.

3.3. Migration kinetics of phosphorus

The process of P migration can be divided into three stages: (1) diffusion of P from the slag to the slag–metal interface, (2) formation of Fe–P compounds at the slag-iron interface, and (3) diffusion of P from the slag–metal interface to the metallic interior. The reduction of iron oxides is much easier than that of apatite in coal-based reduction [25]. Some metal has formed prior to the reduction of apatite. In addition, the content of iron (42.21wt%) in the ore was much greater than that of P (1.31wt%). Thus, an adequate metallic interface was provided for the formation of Fe–P compounds, and the reaction between metallic iron and P was near equilibrium. Therefore, the restrictive step of P migration is not the interface chemical reaction but the diffusion of P in the metal phase.

As shown in Figs. 4 and 5, the P content in the metal phased gradually decreased from the interface to the interior. It was assumed that the concentration gradient primarily provided the driving force for the P diffusion. Moreover, the metallic iron phase existed in the form of a solid-state particle during the reduction. Therefore, Fick's Law was used to derive the P diffusion equation in the metallic phase. According to the P content in the metallic phase at a specified reduction temperature and different time, the diffusion coefficient of P can be calculated and a diffusion kinetics model (i.e., migration kinetics model of P) can be obtained.

Based on Fick's law, the diffusion flux of P in the metallic phase can be expressed as

$$J_{\mathrm{P}} = -D_{\mathrm{P}} \frac{\mathrm{d}c_{\mathrm{P}}}{\mathrm{d}x} \tag{1}$$

where J_{P} is the P diffusion flux (mol·m^{-2}·s^{-1}), D_{p} is the P diffusion coefficient (m^2·s^{-1}), $\mathrm{d}c_{\mathrm{P}}/\mathrm{d}x$ is the P concentration gradient (mol·m^{-4}). It was assumed that $\mathrm{d}c_{\mathrm{P}}/\mathrm{d}x$ is constant and Eq. (1) can be written as

$$J_{\mathrm{P}} = -D_{\mathrm{P}} \frac{c_{\mathrm{P}} - c_{\mathrm{P}}^{\mathrm{I}}}{\Delta x} \tag{2}$$

where c_{p} is the concentration of P in the metallic phase (mol·m^{-3}), $c_{\mathrm{P}}^{\mathrm{I}}$ is the initial concentration of P in the metallic phase (mol·m^{-3}), and Δx is the thickness of the metallic phase (m). Using Eq. (2), the diffusion rate of P in the metallic phase can be expressed as

$$N_{\mathrm{P}} = -J_{\mathrm{P}} A = \frac{AD_{\mathrm{P}}}{\Delta x}\left(c_{\mathrm{P}} - c_{\mathrm{P}}^{\mathrm{I}}\right) \tag{3}$$

where N_{P} is the P diffusion rate (mol·s^{-1}), A is the surface area of the metallic phase (m^2). The increase in the rate of P concentration in the metallic phase can be expressed as

$$\frac{\mathrm{d}c_{\mathrm{P}}}{\mathrm{d}t} = \frac{N_{\mathrm{P}}}{V} \tag{4}$$

where V is the metallic phase volume (m^3), and t is the reaction time (s). Eq. (3) was substituted into Eq. (4), and it can be deduced that

$$\frac{\mathrm{d}c_{\mathrm{P}}}{\mathrm{d}t} = \frac{AD_{\mathrm{P}}}{V\Delta x}\left(c_{\mathrm{P}} - c_{\mathrm{P}}^{\mathrm{I}}\right) \tag{5}$$

By rearranging and integrating, Eq. (5) can be expressed as

$$\ln\frac{c_{\mathrm{P}}^{t} - c_{\mathrm{P}}^{\mathrm{I}}}{c_{\mathrm{P}}^{0} - c_{\mathrm{P}}^{\mathrm{I}}} = \frac{AD_{\mathrm{P}}}{V\Delta x}t \tag{6}$$

where c_{P}^{t} is the average concentration of P in the metallic phase at time t (mol·m^{-3}), and c_{P}^{0} is the initial content of P in slag phase (mol·m^{-3}). Based on previous analysis, metallic iron forms before the reduction of apatite, and thus, the initial concentration of P in the metallic phase is considered to be 0. Therefore, Eq. (6) can be approximated as

$$\ln\frac{c_{\mathrm{P}}^{t}}{c_{\mathrm{P}}^{0}} = \frac{AD_{\mathrm{P}}}{V\Delta x}t \tag{7}$$

The metallic phase existed in the shape of a sphere [26]. Therefore, Eq. (7) can be expressed as

$$\ln\frac{c_P^t}{c_P^0}=\frac{12D_P}{d_t^2}t \tag{8}$$

where d_t is the mean diameter of the metallic phase at time t (m). The value of d_t was obtained from a previous paper [26]. Briefly, the reduced sample was embedded, polished and photographed using an Olympus BX41M metallographic microscope. Then after image analysis using Motic Images Advanced 3.2 software, the particle size of each metallic iron phase was acquired, and the mean size of the metallic phase was calculated by the following equation.

$$\overline{d}=\frac{\sum_{i=1}^{N}d_i}{N} \tag{9}$$

where $\overline{d}$ is the mean grain size of the metallic iron, N is the total number of metallic iron grains (dimensionless), and d_i is the size of each metallic iron phase (μm).

Using the mass content of P, Eq. (8) can be transformed into

$$\ln\frac{w_P^t}{w_P^0}=\frac{12D_P}{d_t^2}t \tag{10}$$

where w_P^t is the mass content of P in the metallic phase at time t (%). w_P^0 is the mass content of P in the slag phase at the initial moment. The values of D_p can be determined from the slopes of the linear regression of $\ln(w_P^t/w_P^0)$ versus t and the corresponding d_t. During reduction, iron oxides were reduced to metallic iron, gangue minerals in iron ore and ash in coal formed slag phase. In order to determine w_P^0, it was assumed that the initial slag was generated just from the gangue minerals and ash, and not from the iron oxides. Therefore, according to the composition of iron ore and coal (Tables 1 and 2) and dosage of coal, the w_P^0 was 3.42wt%.

The average content of P (w_P^t) was calculated by the P content at different positions in the metallic phase, as shown in Fig. 5. The plots of $\ln(w_P^t/w_P^0)$ versus t are presented in Fig. 6. Evidently, $\ln(w_P^t/w_P^0)$ and t presented good linearity, which indicates that calculating the diffusion coefficient of P using Eq. (10) was feasible. The calculated diffusion coefficients of P under different conditions are presented in Table 4. The diffusion coefficient of P in the metallic phase varied between 3.81×10^{-15}–7.62×10^{-15} $m^2\cdot s^{-1}$. Additionally, the diffusion coefficient of P gradually increased with an increase in reduction time and temperature. For example, when oolitic iron ore was reduced at 1498 K for 10 to 80 min, the diffusion coefficient of P increased from 4.07×10^{-15} $m^2\cdot s^{-1}$ to 7.29×10^{-15} $m^2\cdot s^{-1}$. At a reduction time of 30 min, the diffusion coefficient of P increased from 4.55×10^{-15} $m^2\cdot s^{-1}$ to 5.24×10^{-15} $m^2\cdot s^{-1}$ when the reduction temperature increased from 1473 to 1548K. This was attributed to the reduction of apatite being accelerated at high temperatures and long reduction times, providing more reduced P for diffusion.

Table 4. Diffusion coefficients of phosphorus in the metallic phase

Temperature / K	D_P / (10^{-15} $m^2\cdot s^{-1}$)						
	10 min	20 min	30 min	40 min	60 min	80 min	Mean value
1473	3.81	4.17	4.55	4.98	6.28	7.18	5.16
1498	4.07	4.45	4.69	4.91	6.38	7.29	5.30
1523	4.29	4.66	5.04	5.31	6.46	7.49	5.54
1548	4.40	4.95	5.24	5.58	6.57	7.62	5.73

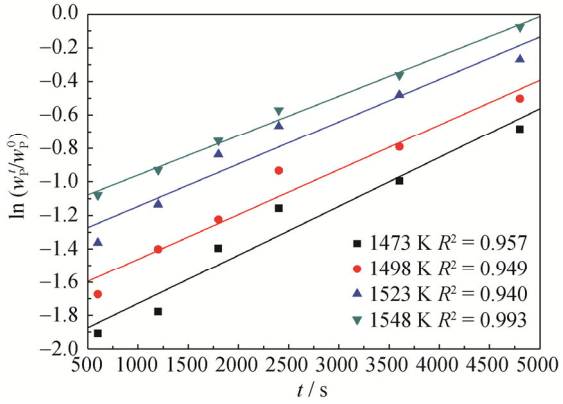

Fig. 6. Plots of $\ln(w_P^t/w_P^0)$ versus t for phosphorus migration at various reduction temperatures.

The relationship between diffusion coefficient and temperature follows the Arrhenius equation, expressed as

$$D=D_0\exp\left(-\frac{Q}{RT}\right) \tag{11}$$

where D is the diffusion coefficient ($m^2\cdot s^{-1}$), D_0 is the diffusion constant ($m^2\cdot s^{-1}$), Q is the diffusion activation energy ($J\cdot mol^{-1}$), R is the gas constant (8.314 $J\cdot mol^{-1}\cdot K^{-1}$), and T is the temperature (K). Taking the natural logarithm of both sides, Eq. (11) can be expressed as

$$\ln D=\ln D_0-\frac{Q}{RT} \tag{12}$$

The value of the diffusion activation energy (Q) and diffusion constant (D_0) can be determined from the slopes and intercept of the linear regression of ln$D$ versus $1/T$.

The mean diffusion coefficient in Table 4 was used to calculate the diffusion activation energy and diffusion constant, and the plot of ln$D$ versus $1/T$ is shown in Fig. 7. The linear fitting of ln$D$ versus $1/T$ presented good linearity, which indicated that the relationship of the diffusion coefficient with temperature is in good agreement with the Arrhenius equation. According to the slope of the regression line, the diffusion activation energy (Q) of P in the metallic phase was 26.96 kJ·mol^{-1}, and the diffusion constant (D_0) was 4.65 × 10^{-14} m^2·s^{-1}. In general, when the diffusion activation energy Q is less than 150 kJ·mol^{-1}, the transfer process is controlled by mass diffusion. The diffusion activation energy for components in metallic iron is usually 17–85 kJ·mol^{-1}. The diffusion activation energy of P in the metallic phase was 26.96 kJ·mol^{-1}, less than 150 kJ·mol^{-1} and within the range of diffusion activation energy for components in metallic iron. Therefore, the calculated value of diffusion activation energy further proved that the migration of P was restricted by diffusion in the metallic phase.

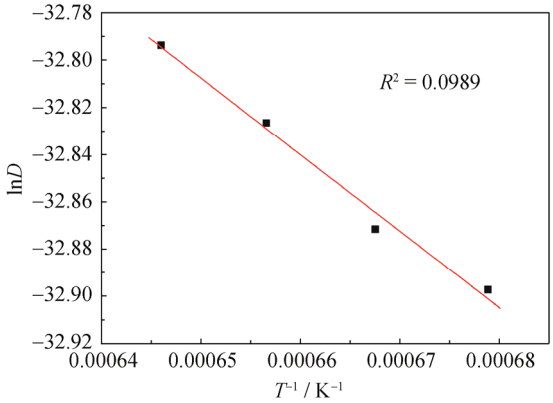

Fig. 7. Dependence of ln$D$ on $1/T$.

Using the calculated diffusion activation energy (Q) and diffusion constant (D_0), the diffusion equation of P in the metallic phase was obtained, and this equation is just the migration kinetics model of P in the coal-based reduction of high-phosphorus oolitic iron ore.

$$N_{\mathrm{P}}^{t} = 9.30\times10^{-14}\pi d_t \exp\left(-\frac{26.96\times10^{3}}{RT}\right)c_{\mathrm{P}}^{t} \quad (13)$$

4. Conclusions

The migration direction of P during coal-based reduction of high-phosphorus oolitic iron ore was from the slag to the metallic phase. The P migration route was as follows: the reduced P diffused from the slag phase to the slag–metal interface, reacted with metallic iron to form Fe–P compounds, and then diffused to the interior of the metallic phase. The reduction time and the temperature showed a significant influence on the P content of the metallic and the slag phases. With increasing reduction temperature and time, the P content at the same test position in the slag phase gradually decreased, while that in the metallic phase clearly increased. The P content in the metallic or slag phase similarly varied with a change in the detected position. In the metallic phase, the P content gradually decreased from the boundary to the interior, while in the slag phase, the P content gradually increased from the interior to the slag–metal interface. The migration kinetics model for P was proposed and described as $N_{\mathrm{P}}^{t} = 9.30\times10^{-14}\pi d_t \exp\left(-\frac{26.96\times10^{3}}{RT}\right)C_{\mathrm{P}}^{t}$. The migration of P during reduction was restricted by the P diffusion in metallic phase.

Acknowledgement

This work was financially supported by the National Natural Science Foundation of China (No. 51604063).

References

[1] J.W. Cha, D.Y. Kim, and S.M. Jung, Distribution behavior of phosphorus and metallization of iron oxide in carbothermic reduction of high-phosphorus iron ore, *Metall. Mater. Trans. B*, 46(2015), No. 5, p. 2165.

[2] W. Yu, T.C. Sun, and T.Y. Hu, Desulfuration behavior of low-grade iron ore-coal briquette during the process of direct reduction followed by magnetic separation, *ISIJ Int.*, 55(2015), No.1, p. 329.

[3] M.I. Abro, A.G. Pathan, and A.H. Mallah, Liberation of oolitic hematite grains from iron ore, Dilband Mines Pakistan, *Mehran Univ. Res. J. Eng. Technol.*, 30(2011), No. 2, p. 329.

[4] S.X. Song, E.F. Campos-Toro, Y.M. Zhang, and A. Lopez-Valdivieso, Morphological and mineralogical characterizations of oolitic iron ore in the Exi region, China, *Int. J. Miner. Metall. Mater.*, 20(2013), No. 2, p. 113.

[5] G.H. Li, S.H. Zhang, M.J. Rao, Y.B. Zhang, and T. Jiang, Effects of sodium salts on reduction roasting and Fe–P separation of high-phosphorus oolitic hematite ore, *Int. J. Miner. Process.*, 124(2013), p. 26.

[6] W. Yu, T.C. Sun, Z.Z. Liu, J. Kou, and C.Y. Xu, Effects of particle sizes of iron ore and coal on the strength and reduction of high phosphorus oolitic hematite-coal composite briquettes, *ISIJ Int.*, 54(2014), No. 1. p. 56.

[7] J. Wu, Z.J. Wen, and M.J. Cen, Development of technologies for high phosphorus oolitic hematite utilization, *Steel Res. Int.*, 82(2011), No. 5, p. 494.

[8] A.P.L. Nunes, C.L.L. Pinto, G.E.S. Valadão, and P.R. de Magalhães Viana, Floatability studies of wavellite and pre-

liminary results on phosphorus removal from a Brazilian iron ore by froth flotation, *Miner. Eng.*, 39(2012), p. 206.

[9] W. Yan, Y.S. Zhang, and Y.C. Liu, Flotation research on a high phosphorus-bearing oolitic hematite ore in Erxi, *China Min. Mag.*, 20(2011), No. 11, p. 71.

[10] P. Delvasto, A. Valverde, A. Ballester, J.A. Muñoz, F. González, M.L. Blázquez, J.M. Igual, and C. García-Balboa, Diversity and activity of phosphate bioleaching bacteria from a high-phosphorus iron ore, *Hydrometallurgy*, 92(2008), No. 3-4, p. 124.

[11] H.H. Wang, G.Q. Li, D. Zhao, J.H. Ma, and J. Yang, Dephosphorization of high phosphorus oolitic hematite by acid leaching and the leaching kinetics, *Hydrometallurgy*, 171(2017), p. 61.

[12] W.T. Xia, Z.D. Ren, and Y.F. Gao, Removal of phosphorus from high phosphorus iron ores by selective HCl leaching method, *J. Iron. Steel Res. Int.*, 18(2011), No. 5, p. 1.

[13] E. Matinde and M. Hino, Dephosphorization treatment of high phosphorus iron ore by pre-reduction, air jet milling and screening methods, *ISIJ Int*., 51(2011), No. 4, p. 544.

[14] Y.F. Yu and C.Y. Qi, Magnetizing roasting mechanism and effective ore dressing process for oolitic hematite ore, *J. Wuhan Univ. Technol. Mater. Sci. Ed*., 26(2011), No. 2, p. 176.

[15] Y.S. Sun, Y.X. Han, P. Gao, Z.H. Wang, and D.Z. Ren, Recovery of iron from high phosphorus oolitic iron ore using coal-based reduction followed by magnetic separation, *Int. J. Miner. Metall. Mater.*, 20(2013), No. 5, p. 411.

[16] K.Q. Li, W. Ni, M. Zhu, M.J. Zheng, and L. Yuan, Iron extraction from oolitic iron ore by a deep reduction process, *J. Iron. Steel Res. Int*., 18(2011), No. 8, p. 9.

[17] W. Yu, T.C. Sun, J. Kou, Y.X. Wei, C.Y. Xu, and Z.Z. Liu, The function of $Ca(OH)_2$ and Na_2CO_3 as additive on the reduction of high-phosphorus oolitic hematite-coal mixed pellets, *ISIJ Int*., 53(2013), No. 3, p. 427.

[18] G.H. Li, M.J. Rao, C.Z. Ouyang, S.H. Zhang, Z.W. Peng, and T. Jiang, Distribution characteristics of phosphorus in the metallic iron during solid-state reductive roasting of oolitic hematite ore, *ISIJ Int*., 55(2015), No. 11, p. 2304.

[19] M.J. Rao, C.Z. Ouyang, G.H. Li, S.H. Zhang, Y.B. Zhang, and T. Jiang, Behavior of phosphorus during the carbothermic reduction of phosphorus-rich oolitic hematite ore in the presence of Na_2SO_4, *Int. J. Miner. Process*., 143(2015), p. 72.

[20] C.C. Yang, D.Q. Zhu, J. Pan, and L.M. Lu, Simultaneous recovery of iron and phosphorus from a high-phosphorus oolitic iron ore to prepare Fe–P alloy for high-phosphorus steel production, *JOM*, 69(2017), No. 9, p. 1663.

[21] Y.S. Sun, Q. Zhang, Y.X. Han, P. Gao, and G.F. Li, Comprehensive utilization of iron and phosphorus from high-phosphorus refractory iron ore, *JOM*, 70(2018), No. 2, p. 144.

[22] G.F. Li, Y.X. Han, P. Gao, and Y.S. Sun, Enrichment of phosphorus in reduced iron during coal based reduction of high phosphorus-containing oolitic hematite ore, *Ironmaking Steelmaking*, 43(2016), No. 3, p. 163.

[23] Y.X. Han, G.F. Li, P. Gao, and Y.S. Sun, Reduction behaviour of apatite in oolitic haematite ore using coal as a reductant, *Ironmaking Steelmaking*, 44(2017), No. 4, p. 287.

[24] P. Gao, G.F. Li, Y.X. Han, and Y.S. Sun, Reaction behavior of phosphorus in coal-based reduction of an oolitic hematite ore and pre-dephosphorization of reduced iron, *Metals*, 6(2016), No. 4, p. 82.

[25] W. Yu, Q.Y. Tang, J.A. Chen, and T.C. Sun, Thermodynamic analysis of the carbothermic reduction of a high-phosphorus oolitic iron ore by FactSage, *Int. J. Miner. Metall. Mater.*, 23(2016), No. 10, p. 1126.

[26] Y.S. Sun, Y.X. Han, P. Gao, and Y.J. Li, Growth kinetics of metallic iron phase in coal-based reduction of oolitic iron ore, *ISIJ Int.*, 56(2016), No. 10, p. 1697.